RSC Advances


This is an *Accepted Manuscript*, which has been through the Royal Society of Chemistry peer review process and has been accepted for publication.

*Accepted Manuscripts* are published online shortly after acceptance, before technical editing, formatting and proof reading. Using this free service, authors can make their results available to the community, in citable form, before we publish the edited article. This *Accepted Manuscript* will be replaced by the edited, formatted and paginated article as soon as this is available.

You can find more information about *Accepted Manuscripts* in the Information for Authors.

Please note that technical editing may introduce minor changes to the text and/or graphics, which may alter content. The journal's standard Terms & Conditions and the Ethical guidelines still apply. In no event shall the Royal Society of Chemistry be held responsible for any errors or omissions in this *Accepted Manuscript* or any consequences arising from the use of any information it contains.

ROYAL SOCIETY OF CHEMISTRY

www.rsc.org/advances

# On the morphology of $MoS_2$ slabs on $MoS_2/Al_2O_3$ catalysts: the influence of Mo loading

Jianjun Chen[1]*, Laetitia Oliviero[1], Xavier Portier[2], Françoise Maugé[1]

1. Laboratoire Catalyse et Spectrochimie, ENSICAEN, Université de Caen, CNRS, 6 bd du Maréchal Juin, 14050 Caen, France
2. CIMAP, ENSICAEN, Université de Caen, CNRS, CEA, 6 bd du Maréchal Juin, 14050 Caen, France

*Corresponding author: jianjun.chen@ensicaen.fr

Abstract: The two-dimensional $MoS_2$ is an important material with diverse catalytic applications. The edge sites exposed by $MoS_2$ are of great importance to its catalytic performance since the catalytic reactions generally occur on the edge sites rather than on the basal planes. In this work, low temperature (100 K) CO adsorption followed by IR spectroscopy (IR/CO) was used to *in situ* probe the edge sites of $MoS_2$ phase on $MoS_2/Al_2O_3$ catalysts. It is found that the morphology of $MoS_2$ phase on $Al_2O_3$ support is a truncated triangle exposing mainly Mo-terminated edge (M-edge). However, the proportion of sulfur-terminated edge (S-edge) increases with increasing the Mo loading, resulting in a more heavily truncated triangle morphology of $MoS_2$. The change of $MoS_2$ morphology with Mo loading can be explained by the modification of $MoS_2$-$Al_2O_3$ interactions, indicating the importance of phase-support interactions in supported $MoS_2$ catalysts.

Keywords: Molybdenum disulfide ($MoS_2$), Slab morphology, Infrared (IR) spectroscopy, CO adsorption, Metal loading.

RSC Advances Accepted Manuscript

# 1 Introduction

The two-dimensional (2D) Molybdenum sulfide ($MoS_2$) nanostructure (slab) is one of the most important materials with diverse applications. While supported $MoS_2$ is used in traditional hydrodesulfurization (HDS) process to remove sulfur from crude oil feedstock,[1] exciting application of $MoS_2$ was recently found in hydrogen evolution reaction (HER).[2] Since the catalytic reactions usually proceed on the edge sites of $MoS_2$ slabs and the basal planes are generally catalytically inert,[3] the type and number of edges exposed under different synthesis conditions are of crucial importance to $MoS_2$ catalytic performance.

In its perfect crystallographic (100) plane, $MoS_2$ exposes principally two types of edges: the Mo terminated edge (M-edge) and the sulfur terminated edge (S-edge).[4] Recently, it was found that the relative ratio of M-edge and S-edge, i.e. the morphology of $MoS_2$, is strongly influenced by $MoS_2$-support interactions. With STM (scanning tunneling microscopy), Walton and co-workers observed that $MoS_2$ adopts a triangle shape exposing only one edge on Au support, whereas it presents a hexagon shape with both M-edge and S-edge on graphite and $TiO_2$.[5] On the same support of $Al_2O_3$, we recently found that the $MoS_2$ morphology can be stepwise tuned from a slightly truncated triangle to a heavily truncated triangle by addition of chelating agent during catalyst preparation.[6] In addition, DFT simulations show that the ratio of anchored and free edge sites (including the relative proportion of M-edge and S-edge sites) differs with $MoS_2$-support interactions [7].

As an important parameter in supported $MoS_2$ catalysts, the effect of Mo loading on the catalyst structure and activity was intensively investigated.[8-17] While several studies suggest that the $MoS_2$-$Al_2O_3$ interactions may differ with Mo loading, [13, 18, 19] the correlation of Mo



RSC Advances Accepted Manuscript

loading and $MoS_2$ morphology is never considered. Therefore, in this work the effect of Mo loading on the morphology of $MoS_2$ phase on $MoS_2/Al_2O_3$ catalysts is investigated. For this purpose, a series of oxidic $Mo/Al_2O_3$ precursors with different Mo loading was prepared by conventional impregnation method. The $MoS_2/Al_2O_3$ catalysts were obtained by sulfiding the $Mo/Al_2O_3$ precursors with 10% $H_2S/H_2$ at atmospheric pressure or 4.0 MPa. The $MoS_2$ morphologies on these catalysts were determined with IR spectroscopy using CO as probe molecule that adsorbs on $MoS_2$ edge sites at low temperature (100 K).

# 2 Experimental

## 2.1 Catalyst preparation

A set of oxidic $Mo/Al_2O_3$ catalyst precursors with variable Mo loading (6%, 9%, and 12%, wt Mo) was prepared by the one-step pore volume impregnation method. Firstly, variable amount of ammonium heptamolybdate tetrahydrate $(NH_4)_6Mo_7O_{24}.4H_2O$, Acros Organics) for the designed Mo loading was dissolved in 3.30 mL deionized water. Secondly, 3.00 gram of pretreated γ-$Al_2O_3$ support (Sasol, specific surface area of 252 $m^2/g$ and pore volume of 0.84 mL/g, pre-calcined in air at 723K for 2 hours) was added into the solutions and strongly shaken for 2 hours. Finally, the matured slurry is dried at 110 °C for 3 hours and then calcined at 773K for 3 hours under air.

## 2.2 Infrared (IR) spectroscopy characterization

IR characterization was performed on a newly designed setup called CellEx. The CellEx consists of three parts: (i) a stainless steel reactor for catalyst sulfidation and other treatment under different temperatures, pressures and gas phases; (ii) an IR cell equipped with a



RSC Advances Accepted Manuscript

spectrometer for spectroscopic characterization; and (iii) a transfer connection for transferring sample from reactor into IR cell under inert gas. With the CellEx, the catalysts can be treated under different conditions and sequentially *in situ* characterized by IR spectroscopy without any air pollution. More details about CellEx were described in ref. [20]

### 2.2.1 Catalyst sulfidation

Catalyst sulfidation were performed in the stainless steel reactor of CellEx. Catalyst sample was firstly grounded and pressed into self-supporting pellet. The pellet was introduced into the reactor which was then evacuated to 1.33 Pa to remove the air. After that the pellet was sulfided at 0.1 MPa or 4.0 MPa with the following procedure. (i) 0.1MPa sulfidation: firstly, a gas mixture of 0.1 MPa 30 mL.min$^{-1}$ 10%$H_2S/H_2$ (Air Liquide France, $H_2S$: 9.97%±0.3%, v/v) was introduced into the reaction. Then the reactor was heated with a rate of 3 K.min$^{-1}$ to 623 K and maintained for 2 hours. Sequentially, the reactor was flushed with Ar at 623 K and then cooled down to room temperature under Ar. Finally, the sulfided pellet was transferred under Ar to the IR cell for IR characterization. (ii) 4.0MPa sulfidation: the pressure of reactor was firstly increased to 4.0 MPa with 10% $H_2S/H_2$ mixture. Then the reactor was heated with a rate of 3 K.min$^{-1}$ to 623 K and maintained for 2 hours. During this period, the flow rate of $H_2S/H_2$ was fixed at 30 mL/min. After that, the reactor pressure was decreased to atmospheric pressure. Sequentially, the reactor was flushed with Ar at 623 K and then cooled down to room temperature under Ar. Finally, the sulfided pellet was transferred under Ar to the IR cell for IR characterization.

### 2.2.2 Low-temperature CO adsorption followed by IR spectroscopy characterization (IR/CO)

In the IR cell, the sulfided pellet was firstly heated at 6 K.min$^{-1}$ up to 623 K and kept for



RSC Advances Accepted Manuscript

1 hour under evacuation. The final pressure in the IR cell after evacuation should reach $10^{-3}$ Pa. After that, the pellet was cooled down to 100 K for CO adsorption. CO adsorption was performed by introducing small calibrated doses of CO (Air Liquide France, 99.9973%, purified by trapping in liquid nitrogen before use) at different pressures (0.03 ~1.20 μmol of CO) and finally with 133 Pa CO at equilibrium in the IR cell. IR spectra of adsorbed CO were recorded using a Thermo Scientific Nicolet FT-spectrometer equipped with a MCT detector with 256 scans. Note that the graphical resolution is 0.5 $cm^{-1}$. For comparison, all the spectra presented were normalized to a sulfided catalyst pellet of 5 $mg.cm^{-2}$.

The obtained IR spectra were further decomposed with Peakfit V4.12 using "Autofit peak II—Second derivative Methods". Then the concentration of each type of $MoS_2$ edge sites was determined using the molar extinction coefficient of CO adsorbed on M-edge ($\varepsilon_{M\text{-}edge}$) and S-edge ($\varepsilon_{S\text{-}edge}$) previous measured ($\varepsilon_{M\text{-}edge}$ and $\varepsilon_{S\text{-}edge}$ are 20±3 $\mu mol^{-1}.cm$ and 35±9 $\mu mol^{-1}.cm$, respectively[6]). Details for spectral decomposition, $\varepsilon_{M\text{-}edge}$ and $\varepsilon_{S\text{-}edge}$ measurement, and edge site concentration calculation were described in ref.[6].

## 2.3 TEM characterization

Transmission electron microscopy (TEM) was carried out on a JEOL 2010 FEG operated at 200 kV. The catalyst precursors were firstly sulfided with the same procedure as that used in IR/CO characterization. To limit detrimental exposure to air, the sulfided catalysts were unloaded from the sulfidation reactor under argon flow into ethanol. A few drops of a suspension of catalyst were put on a copper grid. Slab length and stacking degree distributions of sulfide slabs were determined manually by measuring at least 300 slabs per sample from the TEM images. All the TEM images were recorded at the same magnification



RSC Advances Accepted Manuscript

and digitized using a 2k x 2k CCD camera. The image treatment was performed using the commercial software from GATAN (DIGITALMICROGRAPH).

# 3 Results

## 3.1 Catalyst characterization

Both the oxidic $Mo/Al_2O_3$ precursor and the sulfide $MoS_2/Al_2O_3$ catalyst were widely characterized in the literature.[21-25] For the oxidic precursors, it is generally agreed that the isolated and tetrahedral coordinated molybdenum oxide species present at low Mo loadings while the hepta- and octamolybdates species increase with increasing Mo loading [23, 24]. The as-prepared oxidic $Mo/Al_2O_3$ samples in this work were characterized by Raman spectroscopy, and such conclusion is confirmed (SI, Figure S1). Due to the good dispersion of $MoS_2$ phase on $Al_2O_3$ support, the X-ray diffraction (XRD) patterns of $MoS_2/Al_2O_3$ samples shows mainly the characteristics of $Al_2O_3$ without or with only weak signals according to crystalline $MoS_2$ phases up to the $MoO_3$ loading around 15wt%.[26-28]

The obtained 9wt% $MoS_2/Al_2O_3$ catalysts were also characterized by the high resolution TEM (Transmission Electron Microscopy). The $MoS_2$ phase is imaged as tiny slabs (Figure 1) with an average length around 2 nm and average stacking around 1.5 layers (Figure 2). On calcined catalyst, the sulfidation pressure has slight effect on the average slab length and the average stacking number (Figure 2 and ref.[29]). Because of the contrast disturbance from alumina support, the HRTEM provides neither the morphology of $MoS_2$ clusters nor the type of edges that $MoS_2$ exposes (Figure 2 and ref.[25]).

RSC Advances Accepted Manuscript

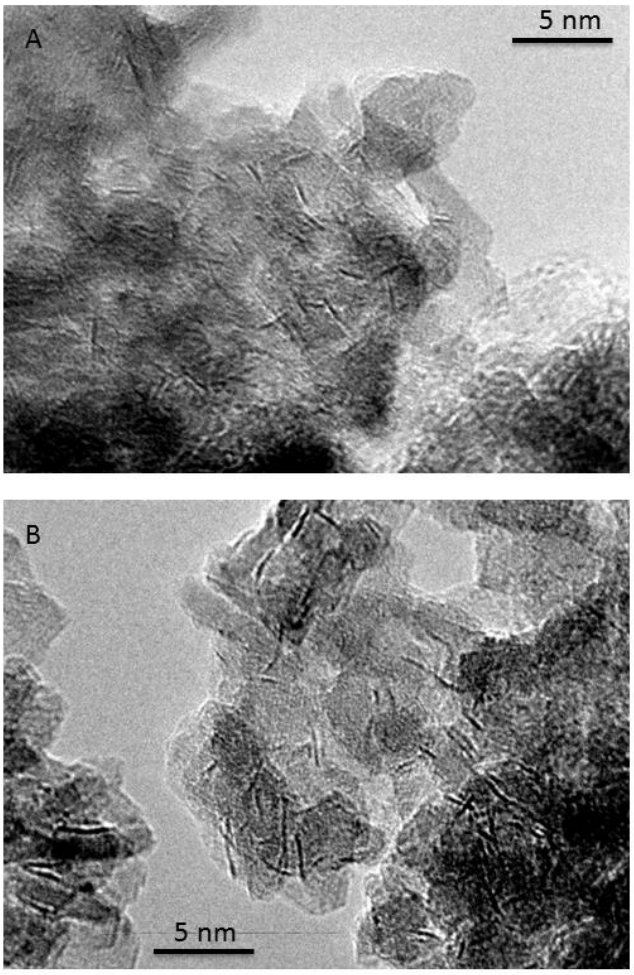


**Figure 1: TEM images of the $MoS_2$ slabs on $MoS_2/Al_2O_3$ catalyst sulfided at 623 K with 0.1 MPa (A) or 4.0 MPa (B) 10% $H_2S/H_2$. The Mo loading is 9wt% on this catalyst.**

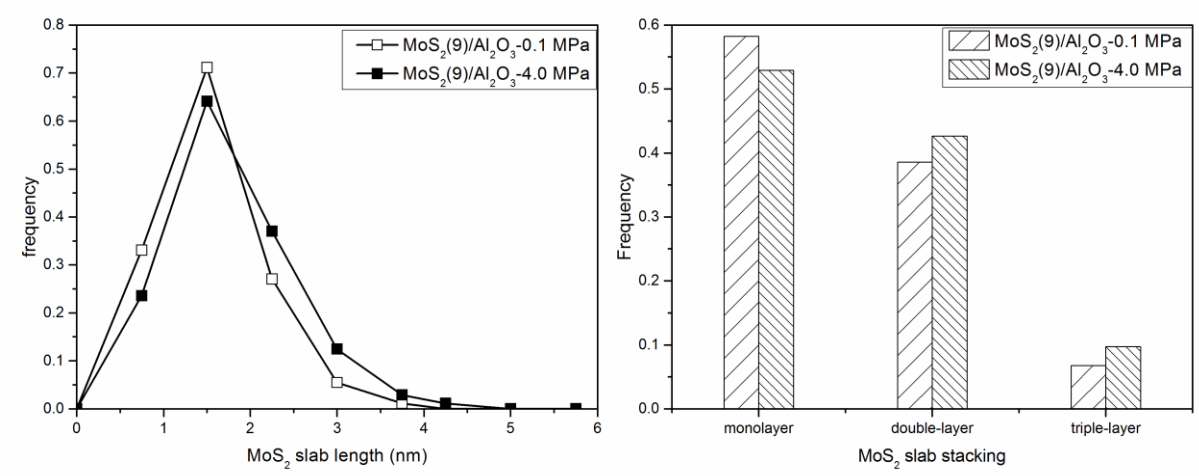


**Figure 2: TEM analysis of the average slab length and stacking of $MoS_2$ on $MoS_2/Al_2O_3$ catalyst sulfided at 623 K with 0.1 MPa or 4.0 MPa 10% $H_2S/H_2$. The Mo loading is 9wt% on this catalyst. The average slab length is 1.9 nm for the 0.1 MPa sulfided catalyst, and 2.2 nm for the 4.0 MPa sulfided one. The average slab stackings are respectively 1.56 (0.1 MPa) and 1.67 (4.0 MPa).**

RSC Advances Accepted Manuscript

## 3.2 IR spectra of low-temperature CO adsorption on $MoS_2/Al_2O_3$ catalyst

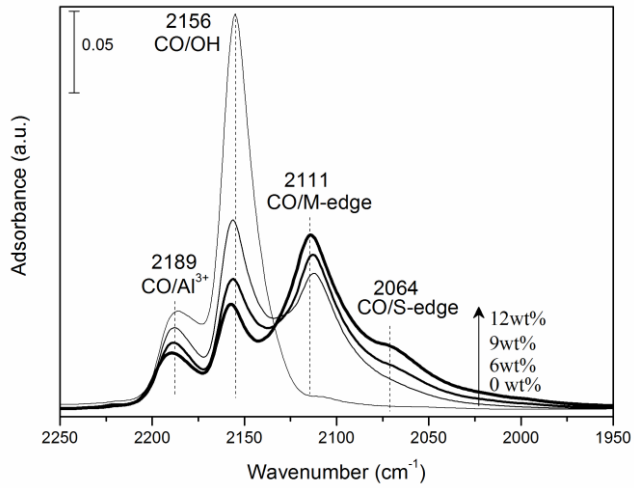


**Figure 3: IR spectra of CO adsorption (133 Pa CO at equilibrium, 100 K) on $MoS_2/Al_2O_3$ prepared with different Mo loading. The $MoS_2/Al_2O_3$ catalysts were obtained by sulfiding the oxidic $Mo/Al_2O_3$ precursors at 623 K and 0.1 MPa with 10% $H_2S/H_2$.**

In order to investigate the $MoS_2$ morphology on $MoS_2/Al_2O_3$ catalyst, low temperature (100 K) CO adsorption followed by IR spectroscopy (IR/CO) was employed to probe the $MoS_2$ edge sites. For comparison, the IR spectrum of CO adsorption on pure $Al_2O_3$ support sulfided by the same procedure is also provided. As shown in Figure 3, low temperature CO adsorption on pure $Al_2O_3$ support leads to two υ (CO) bands located at 2189 and 2156 $cm^{-1}$, which are assigned respectively to CO adsorption on $Al^{3+}$ sites and OH groups on $Al_2O_3$ support.[30] When $MoS_2$ phase is introduced onto $Al_2O_3$ surface, distinct IR/CO bands in the region of 2125-1950 $cm^{-1}$ were observed. The υ (CO) band located at 2111 $cm^{-1}$, as well as the shoulder at 2064 $cm^{-1}$, correspond to CO adsorption on the edge sites of $MoS_2$ phase. Combining experimental IR/CO data with theoretical DFT calculations, Travert and co-workers [31, 32] assigned the former band (~2111 $cm^{-1}$) to CO adsorption on the Mo-terminated edge (M-edge) of $MoS_2$ slabs, and the later one (~2064 $cm^{-1}$) to CO adsorption on the sulfur-terminated edge (S-edge) of $MoS_2$ phase. With increasing Mo



RSC Advances Accepted Manuscript

loading, the intensity of υ (CO) bands on $Al^{3+}$ sites and OH groups stepwise decrease, indicating that more $Al_2O_3$ surface is covered by $MoS_2$ phase, which is in good agreement with the augmentation of Mo loading. Meanwhile, the intensity of υ (CO) bands on both M-edge and S-edge gradually increases, indicating more $MoS_2$ edge sites are formed with the increasing Mo loading. Nevertheless, it should be underlined that these two bands do not increase proportionately. The υ (CO) shoulder band on S-edge becomes more evident with Mo loading.

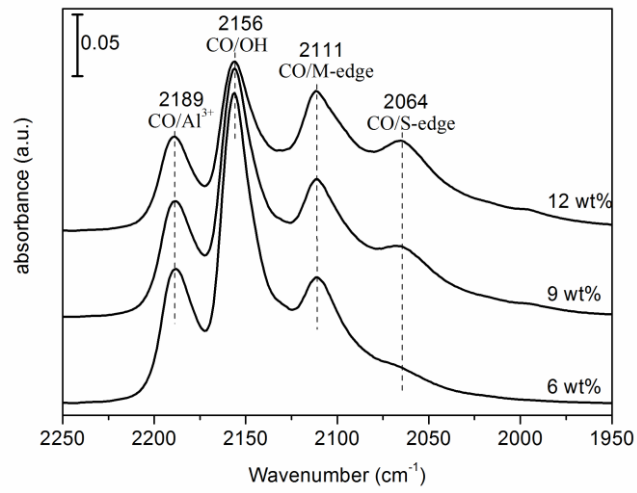


**Figure 4: IR spectra of CO adsorption (133 Pa CO at equilibrium, 100 K) on $MoS_2/Al_2O_3$ prepared with different Mo loading. The $MoS_2/Al_2O_3$ catalysts were obtained by sulfiding the oxidic $Mo/Al_2O_3$ precursors at 623 K and 4.0 MPa with 10% $H_2S/H_2$.**

In order to go further in the parameters that affects the relative change of M-edge and S-edge with Mo loading, the set of oxidic $Mo/Al_2O_3$ precursors were further sulfided with 10% $H_2S/H_2$ at high pressure (4.0 MPa) and then *in situ* characterized by IR/CO. As shown in Figure 4, no new IR band appears on the high pressure sulfided $MoS_2/Al_2O_3$ catalysts. Nevertheless, the υ (CO) band on S-edge (~2064 $cm^{-1}$) is more clearly observed after high pressure sulfidation than after sulfidation at atmospheric pressure. With increasing Mo



RSC Advances Accepted Manuscript

loading, this band is an ill-defined shoulder on 6 wt% $MoS_2/Al_2O_3$ catalyst and becomes a well-defined band on 12 wt% $MoS_2/Al_2O_3$ samples, indicating an increasing of S-edge proportion on the $MoS_2$ phase.

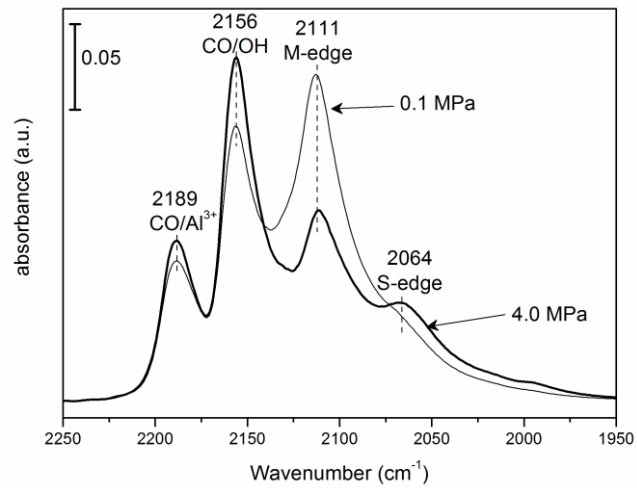


**Figure 5: Comparison of IR spectra of CO adsorption (133 Pa at equilibrium, 100 K) on $MoS_2/Al_2O_3$ sulfided at 623 K with 0.1 MPa (thin line) or 4.0 MPa (bold line) 10% $H_2S/H_2$. The Mo loading is 9 wt% on this catalyst.**

Figure 5 compares the IR/CO spectra on 9wt% $MoS_2/Al_2O_3$ catalysts sulfided at atmospheric (0.1 MPa) and high pressure (4.0 MPa). As can be seen, the CO adsorption intensity on $MoS_2$ phase is strongly modified by sulfidation pressure. With elevating the sulfidation pressure, the CO adsorption intensity on M-edge is decreased, whereas the CO band on S-edge becomes more pronounced. Besides, the CO adsorption intensity on OH groups is also significantly enhanced after high-pressure sulfidation.

RSC Advances Accepted Manuscript

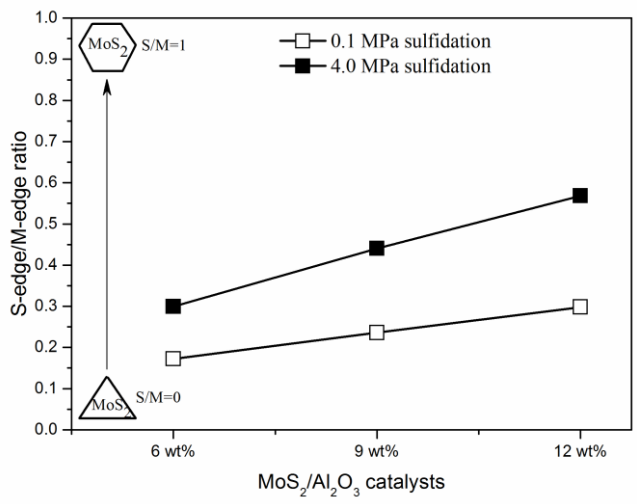


Figure 6: The ratios of S-edge/M-edge on $MoS_2/Al_2O_3$ catalysts as a function of Mo loadings

To depict the $MoS_2$ morphologies on $MoS_2/Al_2O_3$ catalysts, the IR/CO spectra in Figure 3 and Figure 4 were further decomposed with the software Peakfit V4.12 and the concentration of M-edge and S-edge sites detected by low-temperature CO adsorption was calculated. The details for spectral decomposition and sites calculation were reported previously.[6] As shown in Figure 6, the ratio of S-edge/M-edge on the series of $MoS_2/Al_2O_3$ catalysts are steadily increased with Mo loading. Assuming that the ratio of M-edge and S-edge on a single $MoS_2$ slab is in line with the overall ratio of each edge detected by CO adsorption, the data in Figure 6 suggests that with increasing Mo loading, the morphology of $MoS_2$ slabs changes from a slightly truncated triangle exposing mainly M-edge to a more heavily truncated triangle exposing relatively more S-edge. For the same Mo loading, the S-edge/M-edge ratios on the 4.0 MPa sulfided $MoS_2/Al_2O_3$ catalysts are always higher than the ones on the 0.1 MPa sulfided samples, indicating that $MoS_2$ morphology is probably also influenced by sulfidation pressure. Nevertheless, the S-edge/M-edge ratios, even on the high pressure sulfided samples, are much smaller than 1, showing that the $MoS_2$ phase with typical Mo loadings in HDS catalysts mainly exposes M-edge, which is consistent with the DFT



RSC Advances Accepted Manuscript

results that the M-edge is energetically more stable than S-edge under HDS conditions.[33]

# 4 Discussion

## 4.1 On the assignment of CO adsorption bands on $MoS_2$ phase

Although the IR/CO data in this work clearly show that the relative intensity of the two CO adsorption bands on $MoS_2$ phase varies with Mo loading, the conclusion that $MoS_2$ morphology is changed relies firstly on the assignment of the two υ (CO) bands. Besides the M-edge/S-edge assignment used above, another competing assignment in the literature is the edge/corner assignment. By comparison with CO adsorption on metal particles, Muller and co-workers [34] attributed the two υ (CO) bands at 2111 and 2064 $cm^{-1}$ to respectively edge and corner sites of $MoS_2$ slabs. This assignment was used in several studies without further validation.[35, 36] However, this assignment is contradicted with the experimental results present in this paper. Indeed, whatever the morphology of $MoS_2$ slabs is (triangle or hexagon), the corner/edge site ratio should decreases with increasing $MoS_2$ slab size. Since the $MoS_2$ slab size increases with Mo loading,[8, 19, 37, 38], the 2064/2111 υ (CO) band ratio should decreases with increasing Mo loading. However, as shown in Figure 6, the 2064/2111 υ (CO) band ratio steadily increases with increasing Mo loading. Therefore, the assignment of these two bands to CO adsorption on edge and corner sites of $MoS_2$ slabs can be discarded.

Using the density functional method, Zeng and co-workers[39] calculated the CO adsorption on triangular $MoS_x$ clusters. Accordingly, they assigned the *ν*(CO) band at ~2111 $cm^{-1}$ to symmetric coupled stretching of double-CO adsorption on corner site (frequency calculated is 2102 $cm^{-1}$), and the band at ~2064 $cm^{-1}$ to either mono-adsorption stretching or



RSC Advances Accepted Manuscript

asymmetric coupled stretching on the corner site. Firstly, this assignment of double CO adsorption is contradicted with the co-adsorption results of $^{12}CO/^{13}CO$ mixtures on $MoS_2/Al_2O_3$ catalyst.[40, 41] Secondly, the assignment of these two *v*(CO) bands to CO adsorption on corner sites makes it impossible the opposite intensity change of this two bands. However, our recent experimental data on citric acid effect [6] show a decrease of the *v*(CO) band at ~2111 $cm^{-1}$ with an increase of the *v*(CO) band at ~2064 $cm^{-1}$. Therefore, this assignment can also be discarded.

The assignment of CO adsorption on other species, such as Mo carbide, can also be excluded, since the catalysts used in the present work were prepared without any carbon additives and calcined at 773K under air before sulfidation. Another assignment to be considered for these two CO bands is the effect of $MoS_2$ stacking. However, this assignment is unlikely since the relative intensity of the two bands varies significantly while the average stacking of $MoS_2$ slabs stays comparable (Figure 2 and ref. [6]). In the same way, the *v*(CO) band at ~2064 $cm^{-1}$ cannot be attributed to the nanometer-sized entities as observed by Kooyman and co-workers[25], since these nanoparticles, which predominantly occur under mild sulfidation, cannot be the major species on well sulfided $MoS_2/Al_2O_3$ catalyst.

In summary, it is reasonable to assign the two CO adsorption bands at ~2111 and ~2064 $cm^{-1}$ to respectively M-edge and S-edge of $MoS_2$ slabs. The recent work of Labruyere with parallel studies of IR/CO and DFT calculations on the effect of sulfidation temperature confirms again this assignment [42]. Consequently, with this assignment, the IR/CO data presented in this work clearly show that the morphology of $MoS_2$ slab is changed with Mo loading on supported $MoS_2/Al_2O_3$ catalysts.



RSC Advances Accepted Manuscript

## 4.2 The influence of Mo loading on $MoS_2$ morphology

The question of the origin of the $MoS_2$ morphology change with Mo loading arises. Many factors allowed us to interpret this effect by a change in $MoS_2$-$Al_2O_3$ interactions. The $MoS_2$ phase interacts with $Al_2O_3$ support by the so-called Mo-O-Al linkages, which are located at the edges of $MoS_2$ slabs rather than at the bulk sites.[7, 43] Therefore, the concentration of Mo-O-Al linkages (normalized by the total number of Mo in $MoS_2$) will decreases with increasing $MoS_2$ size. Since it is well established in the literature that the $MoS_2$ size increases with Mo loading,[8, 19, 37, 38] the concentration of Mo-O-Al linkages with decreases with increasing Mo loading. Moreover, The Mo-O-Al linkages are formed by the reaction of Mo atoms with hydroxyl groups on $Al_2O_3$ surface.[44] Since the hydroxyl groups on $Al_2O_3$ support have different acidity, the Mo atoms preferentially react with the most basic hydroxyl groups, and the excess Mo atoms will react with less basic or neutral OH groups to form Mo-O-Al linkages.[44] Therefore, the strength of Mo-O-Al linkages also decreases with Mo loading. All these results suggest that the $MoS_2$-$Al_2O_3$ interactions decrease with increasing Mo loading.

According to the Wulff construction,[45] the morphology of $MoS_2$ is determined by the relative free energies of M-edge and S-edge. These edge energies are related to the chemical potential of sulfur in sulfidation,[33] but also sensitive to other parameters such as $MoS_2$-support interactions.[5] The role of $MoS_2$-support interactions on $MoS_2$ morphology can be understood as an extra energy obtained by the edges when interacting with support.[5] We surmise that such additional energy is not the same on M-edge and S-edge. Therefore, the growth of one edge will be promoted, and thus the $MoS_2$ morphology is changed when



RSC Advances Accepted Manuscript

changing $MoS_2$-support interactions.

The above explanations of $MoS_2$ morphology change with Mo loadings are consistent with the previous report. Our previous study on citric acid [6] demonstrated that the reduction of $MoS_2$-$Al_2O_3$ interactions by chelating agent addition promotes the growth of S-edge, thus leading to the morphology change of $MoS_2$ slabs from a slightly truncated triangle exposing mainly M-edge to a hexagon with both M-edge and S-edge. In this paper, the reduction of $MoS_2$-$Al_2O_3$ interactions can also be expected with increasing Mo loadings. Accordingly, it is observed that the $MoS_2$ slabs on $MoS_2/Al_2O_3$ catalysts expose relatively more S-edge with increasing Mo loading.

## 4.3 The effect of high pressure sulfidation

The role of the sulfidation pressure on $MoS_2$ morphology is even more crucial since the effect of Mo loading on morphology is more prominent after 4.0 MPa sulfidation. The results in this work point out that $MoS_2$ morphology is also influenced by the sulfidation pressure since the S-edge/M-edge ratio is always greater on the high pressure sulfided samples for the same Mo loading. According to Le Chatelier's principle, the effect of sulfidation pressure can be tentatively interpreted as that the increase of the total gas phase pressure ($P_{H2S}$+$P_{H2}$) will favor the thiolysis of Mo-O-Al linkages toward the formation of Mo-SH and Al-OH,[46] and thus lowers the $MoS_2$-$Al_2O_3$ interactions. Besides, it was also observed that the CO uptake on the high pressure sulfided $MoS_2$ is lower than that on the atmospheric sulfided one (Figure 5), implying that sulfidation pressure probably also changes the sulfur coverage on $MoS_2$ edge sites as suggested by DFT calculations.[47] The effect of sulfidation pressure on $MoS_2$ morphology and edge structure will be further



RSC Advances Accepted Manuscript

investigated in another work.

# 5 Conclusion

In this work, low temperature CO adsorption followed by IR spectroscopy (IR/CO) is used to demonstrate the $MoS_2$ morphology change with Mo loading on *real* type $MoS_2/Al_2O_3$ catalysts. It is found that the morphology of $MoS_2$ on $Al_2O_3$ support is a truncated triangle exposing both M-edge and S-edge, and that the truncation degree, i.e., ratio of S-edge/M-edge, increases with Mo loading. The effect of Mo loading on $MoS_2$ morphology can be explained by the modification of $MoS_2$-$Al_2O_3$ interactions. Nevertheless, because of the strong interactions between $MoS_2$ and $Al_2O_3$ support, $MoS_2$ presents mainly M-edge rather than S-edge even at high Mo loading and high pressure sulfidation, indicating that M-edge is energetically much more stable than S-edge on $Al_2O_3$ support.

# Acknowledgements

The French Ministry of Research is acknowledged for the Ph. D. grant of J. Chen. Yoann Levaque, Valérie Ruaux, and Philippe Bazin are greatly acknowledged for the technical support on IR experiment. Guillaume CLET is greatly acknowledged for the Raman characterization. Xavier PORTIER is greatly acknowledged for the TEM analysis.

# References

1. H. Topsoe, B. S. Clausen and F. E. Massoth, *Hydrotreating catalysis*, Springer, Berlin-Heidelberg, 1996.
2. I. Song, C. Park and H. C. Choi, *RSC Adv.*, 2015, **5**, 7495-7514.
3. T. F. Jaramillo, K. P. Jorgensen, J. Bonde, J. H. Nielsen, S. Horch and I. Chorkendorff, *Science*, 2007, **317**, 100-102.
4. J. V. Lauritsen, J. Kibsgaard, S. Helveg, H. Topsoe, B. S. Clausen, E. Laegsgaard and F. Besenbacher, *Nat. Nanotechnol.*, 2007, **2**, 53-58.
5. A. S. Walton, J. V. Lauritsen, H. Topsoe and F. Besenbacher, *J. Catal.*, 2013, **308**, 306-318.
6. J. Chen, F. Maugé, J. El Fallah and L. Oliviero, *J. Catal.*, 2014, **320**, 170-179.



RSC Advances Accepted Manuscript

7. D. Costa, C. Arrouvel, M. Breysse, H. Toulhoat and P. Raybaud, *J. Catal.*, 2007, **246**, 325-343.
8. L. Jalowiecki-Duhamel, J. Grimblot and J. P. Bonnelle, *J. Catal.*, 1991, **129**, 511-518.
9. E. Etienne, E. Ponthieu, E. Payen and J. Grimblot, *J. Non -Cryst. Solids.*, 1992, **147-148**, 764-768.
10. Y. Yokoyama, N. Ishikawa, K. Nakanishi, K. Satoh, A. Nishijima, H. Shimada, N. Matsubayashi and M. Nomura, *Catal. Today*, 1996, **29**, 261-266.
11. R. Iwamoto and J. Grimblot, *Stud. Surf. Sci. Catal.*, 1997, **106**, 195-210.
12. R. Iwamoto and J. Grimblot, *Stud. Surf. Sci. Catal.*, 1999, **121**, 289-294.
13. E. J. M. Hensen, V. H. J. de Beer, J. A. R. van Veen and R. A. van Santen, *Catal. Lett.*, 2002, **84**, 59-67.
14. A. Ishihara, F. Dumeignil, D. H. Wang, X. G. Li, H. Arakawa, E. W. Qian, S. Inoue, A. Muto and T. Kabe, *Appl. Catal. A*, 2005, **292**, 50-60.
15. P. Blanchard, C. Lamonier, A. Griboval and E. Payen, *Appl. Catal., A*, 2007, **322**, 33-45.
16. A. Ishihara, *J. Jpn. Petrol. Inst.*, 2008, **51**, 73-82.
17. J. Mazurelle, C. Lamonier, C. Lancelot, E. Payen, C. Pichon and D. Guillaume, *Catal. Today*, 2008, **130**, 41-49.
18. P. Arnoldy, J. A. M. Vandenheijkant, G. D. Debok and J. A. Moulijn, *J. Catal.*, 1985, **92**, 35-55.
19. H. Shimada, N. Matsubayashi, T. Sato, Y. Yoshimura, M. Imamura, T. Kameoka and A. Nishijima, *Catal. Lett.*, 1993, **20**, 81-86.
20. L. Oliviero, L. Mariey, M.-A. Lelias, S. Aiello, J. van Gestel and F. Mauge, *Catal. Lett.*, 2010, **135**, 62-67.
21. G. M. Dhar, B. N. Srinivas, M. S. Rana, M. Kumar and S. K. Maity, *Catal. Today*, 2003, **86**, 45-60.
22. G. Mestl and T. K. K. Srinivasan, *Catal. Rev. - Sci. Eng.*, 1998, **40**, 451-570.
23. H. C. Hu, I. E. Wachs and S. R. Bare, *J. Phys. Chem.*, 1995, **99**, 10897-10910.
24. K. V. R. Chary, K. R. Reddy, G. Kishan, J. W. Niemantsverdriet and G. Mestl, *J. Catal.*, 2004, **226**, 283-291.
25. P. J. Kooyman, E. J. M. Hensen, A. M. de Jong, J. W. Niemantsverdriet and J. A. R. van Veen, *Catal. Lett.*, 2001, **74**, 49-53.
26. B. Liu, Y. M. Chai, Y. P. Li, A. J. Wang, Y. Q. Liu and C. G. Liu, *Appl. Catal. A*, 2014, **471**, 70-79.
27. W. B. Chen, F. Mauge, J. van Gestel, H. Nie, D. D. Li and X. Y. Long, *J. Catal.*, 2013, **304**, 47-62.
28. D. Liu, Z. Li, Q. Sun, X. Kong, A. Zhao and Z. Wang, *Fuel*, 2012, **92**, 77-83.
29. A. I. Dugulan, E. J. M. Hensen and J. A. R. van Veen, *Catal. Today*, 2008, **130**, 126-134.
30. K. I. Hadjiivanov and G. N. Vayssilov, *Adv. Catal.*, 2002, **47**, 307-511.
31. A. Travert, C. Dujardin, F. Mauge, S. Cristol, J. F. Paul, E. Payen and D. Bougeard, *Catal. Today*, 2001, **70**, 255-269.
32. A. Travert, C. Dujardin, F. Mauge, E. Veilly, S. Cristol, J. F. Paul and E. Payen, *J. Phys. Chem. B*, 2006, **110**, 1261-1270.
33. H. Schweiger, P. Raybaud, G. Kresse and H. Toulhoat, *J. Catal.*, 2002, **207**, 76-87.
34. B. Muller, A. D. Vanlangeveld, J. A. Moulijn and H. Knozinger, *J. Phys. Chem.*, 1993, **97**, 9028-9033.
35. L. P. A. F. Elst, S. Eijsbouts, A. D. van Langeveld and J. A. Moulijn, *J. Catal.*, 2000, **196**, 95-103.
36. F. Cesano, S. Bertarione, A. Piovano, G. Agostini, M. M. Rahman, E. Groppo, F. Bonino, D. Scarano, C. Lamberti, S. Bordiga, L. Montanari, L. Bonoldi, R. Millini and A. Zecchina, *Catal. Sci. Technol.*, 2011, **1**, 123-136.
37. Y. P. Li, A. T. Li, F. F. Li, D. P. Liu, Y. M. Chai and C. G. Liu, *J. Catal.*, 2014, **317**, 240-252.
38. E. Payen, S. Kasztelan, S. Houssenbay, R. Szymanski and J. Grimblot, *J. Phys. Chem.*, 1989, **93**, 6501-6506.
39. T. Zeng, X. D. Wen, Y. W. Li and H. J. Jiao, *J. Phys. Chem. B*, 2005, **109**, 13704-13710.


RSC Advances Accepted Manuscript

40. M. A. Lelias, A. Travert, J. van Gestel and F. Mauge, *J. Phys. Chem. B*, 2006, **110**, 14001-14003.
41. X.-D. Wen, T. Zeng and H. Jiao, *J. Phys. Chem. B*, 2006, **110**, 14004-14005.
42. V. Labruyere, Ph.D thesis, Universite of Caen, 2014.
43. C. Arrouvel, M. Breysse, H. Toulhoat and P. Raybaud, *J. Catal.*, 2005, **232**, 161-178.
44. N. Y. Topsoe and H. Topsoe, *J. Catal.*, 1993, **139**, 631-640.
45. G. Wulff, *Z. Krystallogr. Minera.*, 1901, **34**, 449-530.
46. Y. V. Joshi, P. Ghosh, M. Daage and W. N. Delgass, *J. Catal.*, 2008, **257**, 71-80.
47. P. Y. Prodhomme, P. Raybaud and H. Toulhoat, *J. Catal.*, 2011, **280**, 178-195.

RSC Advances Accepted Manuscript